Journal of Building Engineering 114 (2025) 114379

Contents lists available at ScienceDirect

Journal of Building Engineering

journal homepage: www.elsevier.com/locate/jobe

Reactivity of olivine-derived amorphous silica and its potential for use as a supplementary cementitious material

Jean Noel Yankwa Djobo *, Sam Draper, Barney Shanks, Hong Wong, Christopher Cheeseman

Centre for Infrastructure Materials, Department of Civil and Environmental Engineering, Imperial College London, SW7 2AZ, United Kingdom

ARTICLE INFO

Keywords:
Olivine
Silica
Low-carbon cement
Hydration mechanism
Compressive strength

ABSTRACT

Traditional supplementary cementitious materials (SCM) are declining in availability because of ongoing transitions in the energy and steel sectors. Olivine is a globally abundant mineral that can be processed to produce low-carbon amorphous silica (APS) with the potential for use as an SCM. This study aims to investigate the reactivity of olivine-derived silica during cement hydration, to optimise its use in concrete. Portland cement pastes at a 0.5 water-to-binder (w/b) ratio with up to 20 wt% APS and up to 4 wt% gypsum, for sulfate adjustment, were assessed. Samples were tested for pozzolanic reactivity, hydration kinetics and phase assemblage using the R^3 test, isothermal calorimetry, quantitative XRD and TGA. Mortar samples at a 0.63 w/b ratio containing up to 40 wt% APS were produced for assessing workability and compressive strength development. The results show that APS is highly reactive. High specific surface area and a porous structure promote early sulfate depletion, workability loss and delayed hydration. The dilution effect dominates the early age hydration, resulting in low strengths compared to the control sample. However, additional gypsum can mitigate these undesirable effects by improving the degree of hydration and early age strengths. APS promotes pozzolanic reactions and strength gain over time, achieving compressive strengths ~50 MPa at 90 days for 20 wt% APS, which exceeds the control.

1. Introduction

Developing low-carbon construction materials is an important lever in the road map to achieve global net-zero emissions by 2050 [1]. Portland cement production is responsible for approximately 8 % of global CO_2 emissions, and this is expected to increase because of the substantial volume of cement required to meet future demand [2]. CO_2 is released during cement manufacturing from the decomposition of limestone, a key raw material, making complete decarbonization of cement particularly challenging. The partial replacement of cement with supplementary cementitious materials (SCMs) in a binary or ternary system is an approach to mitigate emissions from cement production [3–5].

The main SCMs currently used are blast furnace slag and coal fly ash, which are by-products from the steel industry and coal power generation, respectively [6,7]. However, these materials have significant supply issues due to the transition to recycled steel and the move to alternative energy sources such as solar, wind, and geothermal. Clay is a widely abundant resource but has poor reactivity and

* Corresponding author.
E-mail addresses: noel.djobo@imperial.ac.uk, noeldjobo@gmail.com (J.N.Y. Djobo).

https://doi.org/10.1016/j.jobe.2025.114379
Received 3 March 2025; Received in revised form 1 October 2025; Accepted 11 October 2025
Available online 13 October 2025

needs to be calcined at temperatures up to 950 °C, depending on the clay type, to exhibit good pozzolanic reactivity. Volcanic ash is a naturally occurring pozzolan, but it has limited availability [8].

Carbon capture and storage/utilisation (CCS/U) has been proposed as a major pathway to achieving net-zero cement production. This involves capturing carbon released from the kiln, followed by geological sequestration (CCS) or conversion into products (CCU) [9,10]. Advances in this field have led to several innovative approaches. An example is direct or indirect CO_2 sequestration by abundant magnesium silicate minerals, such as olivine, through mineralisation in magnesium carbonate and precipitation of silica [11–13]. Depending on the dissolution and separation technique applied, silica of different purity, crystallinity and textural properties can be obtained, and the carbon footprint may be neutral or negative [14–16].

Olivine-derived silica is generally amorphous, with high specific surface area and high reactivity [9,17,18]. The use of materials with high specific surface area as an SCM increases water demand and decreases workability [19]. The SCM can also change the hydration behaviour of clinker phases by accelerating sulfate depletion and aluminate hydration and potentially affecting mechanical properties [20]. This research examines how olivine-derived silica interacts with cement hydration, focusing on its effects on reaction kinetics, workability, phase assemblage, and compressive strength. The goal is to optimise its use as a supplementary cementitious material (SCM) for low-carbon concrete. While comparisons to other SCMs are useful, this study centres on the fundamental reactivity and performance of olivine-derived amorphous silica as groundwork for future analyses.

2. Materials and methods

2.1. Cementitious materials and characteristics

Ordinary Portland cement class CEM I 52.5N was used with amorphous precipitated silica (APS) recovered from olivine as SCM. The APS was prepared following the procedure previously described in Refs. [9,10]. The process involves the digestion of olivine ($(Mg,Fe)_2SiO_4$, supplied by Sibelco Nordic AS) in diluted sulfuric acid (H_2SO_4, 98 wt%, from VWR) at 70 °C for 2 h. A mass ratio of olivine to sulfuric acid solution (3M) of 6.5 was used. After dissolution, isopropanol (IPA, 99 wt%, Sigma-Aldrich) was added to induce liquid-liquid phase separation. The slurry separates into an upper layer containing precipitated silica gel and a lower layer containing green magnesium/iron sulfate solution. The silica gel was extracted using a 0.5 mm sieve and then dried at 70 °C to remove excess IPA. It was then washed in tap water until the leachate became clear. This was to ensure that all impurities, including dissolved species and acid solution, were removed. The final stage consists of drying the APS at 105 °C. Our previous study reported that the carbon benefits of APS production can reach ~1.5 tonnes eCO_2 removed per tonne of APS produced, given that the slurry (magnesium/iron sulfate) is utilised for carbon capture and storage and a green energy source is employed [9].

Table 1 reports on the chemical composition and physical properties of olivine, APS and cement. The chemical composition was determined using X-ray fluorescence (XRF, Malvern Panalytical Zetium). The specific surface area was obtained using N_2 adsorption (Micromeritics 3Flex), and the density was measured using a helium pycnometer (Micromeritics AccuPyc II 1340). The particle size analysis was completed using laser diffraction (Malvern Panalytical Mastersizer 3000) with water as the dispersant. X-ray diffraction (XRD, Malvern Panalytical Empyrean) data of olivine and APS are shown in Fig. 1a. The mineralogical composition of olivine, APS and cement measured using quantitative XRD is presented in Table 2. The APS is rich in SiO_2 (73 wt%) with 15 wt% LOI corresponding to the dehydroxylation of the silanol group and unreacted mineral impurities on heating to 1050 °C for 2 h. The APS is mostly amorphous with clinochlore ($Mg_5Al(AlSi_3O_{10})(OH)_8$) and chabazite ($((Ca,K_2,Na_2)_2[Al_2Si_4O_{12}]_2.12H_2O$) as the main mineral impurities. The APS appears in scanning electron microscopy (SEM) as shown in Fig. 1b, as agglomerates with a porous texture, high surface area and a median diameter of ~28.9 μm.

2.2. Pozzolanic reactivity

The pozzolanic reactivity of APS was assessed using the R^3 test method. A paste consisting of 10 g of APS, 30 g $Ca(OH)_2$, 5 g of $CaCO_3$ and 54 g of potassium solution (4 g/L KOH + 20 g/L K_2SO_4) was prepared as defined in ASTM C1897-20 [21]. 50 g of the paste was loaded into a 125 ml ampoule and placed in an isothermal calorimeter (TA Instruments TAM Air) set at 40 °C. This was chosen to ensure that the thermal signal was within the measurement range of the calorimeter. 31.25 g of water was used as the reference to have the same paste-to-reference mass ratio (1.6) as specified in the standard. Three repeated measurements were recorded to obtain the average cumulative heat release per mass of APS. Thermogravimetry analysis of the hydrated R^3 paste at 3 and 7 days was completed (Netzsch STA 449 F5 Jupiter) under an inert N_2 atmosphere, flowing at the rate of 50 mL/min in the temperature range of 40–1000 °C, using a heating rate of 10 K/min.

2.3. Hydration study

Six blended cement pastes containing varying amounts of APS (0–20 wt%) and gypsum (0–4 wt%) were prepared at a water-to-binder (w/b) mass ratio of 0.5. The mixes are summarised in Table 3, and these were used to study the effect of APS on cement hydration by measuring the heat evolution using isothermal calorimetry at 25 °C (TA Instruments, TAM Air). Commercial-grade gypsum ($CaSO_4.2H_2O$, 99 % purity) from VWR was used as a sulfate carrier to regulate hydration. Each paste was prepared by mixing components for at least 30 s using a vortex mixer. 10 g of the paste was weighed in an ampoule and placed in the calorimeter. Due to the high specific surface area of APS compared to CEM I, a PCE-based superplasticiser (ViscoFlow3000, Sika) was added at 1 wt% to obtain a workable paste. Superplasticisers function by dispersing cement particles through neutralisation of surface charges and reduction of

Table 1
Chemical composition and physical characteristics of the olivine, amorphous precipitated silica (APS) and CEM I.

	Composition (wt.%)										Particle size (μm)			SSA (m^2/g)	Density (g/cm^3)
	SiO_2	Al_2O_3	MgO	CaO	Fe_2O_3	SO_3	Cr_2O_3	Na_2O	LOI	Sum	d_{10}	d_{50}	d_{90}	–	–
Olivine	39.80	0.87	48.71	0.18	6.76	0.85	0.44	0.83	–	98.52	–	–	–	–	–
APS	73.1	1.07	3.35	0.49	1.89	4.00	0.85		15	99.8	6.01	28.9	86.9	146.1	2.14
CEM I	20.3	6.08	1.31	62.1	2.67	3.49	–		1.94	97.8	2.5	14.3	48.3	1.14	3.15

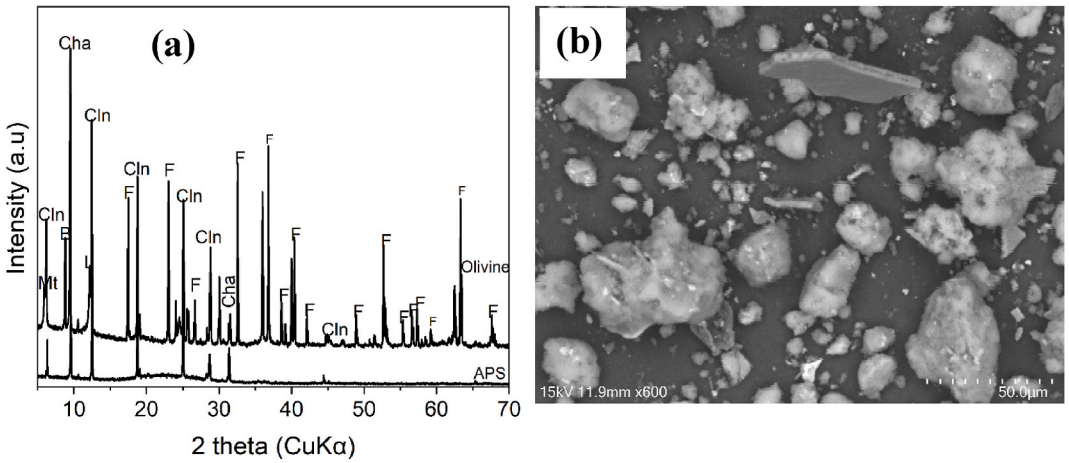

Fig. 1. a) X-ray diffraction pattern of olivine and APS, and b) SEM micrograph of APS. Notation: F = forsterite; Cln = clinochlore; Cha = chabazite; B = biotite; L = lizardite; Mt = montmorillonite.

Table 2
Mineralogical composition of olivine, APS and CEM I from quantitative XRD.

Phase	ICSD	Content (%)		
		Olivine	APS	CEM I
Clinochlore	98-016-4234	18.4	32.3	–
Chabazite	98-002-3913	7.0	14.6	–
Forsterite	98-008-5312	67.0	–	–
Biotite	98-009-5359	2.8	–	–
Lizardite	98-002-3813	4.2	–	–
Montmorillonite	98-016-1171	0.6	–	–
Alite, C_3S	98-002-2501	–	–	60.9
Belite, C_2S	98-024-5077	–	–	8.7
Tricalcium aluminate, C_3A	98-015-1369	–	–	5.0
Brownmillerite, C_4AF	98-005-1266	–	–	1.0
Quartz	98-004-1447	–	–	1.1
Calcite	98-008-8029	–	–	1.6
Anhydrite	98-005-6107	–	–	1.2
Amorphous	–	–	53.2	20.8

Table 3
Mix design of paste and mortar samples.

Mix	Binder (wt. %)			Water/binder ratio	Superplasticiser (wt.% %)	Sand/binder ratio	Flow (mm)
	CEM I	APS	Gypsum				
Paste							
P0	100	–	–	0.5	–	–	–
P10	90	10	–	0.5	1	–	–
P20	80	20	–	0.5	1	–	–
P20-2	78.4	19.6	2	0.5	1	–	–
P20-3	77.6	19.4	3	0.5	1	–	–
P20-4	76.8	19.2	4	0.5	1	–	–
Mortar							
M0	100	–	–	0.63	–	3	163.0 ± 1.9
M10	90	10	–	0.63	2	3	122.3 ± 0.3
M20	80	20	–	0.63	2	3	108.5 ± 1.0
M40	60	40	–	0.63	2	3	100.9 ± 0.7
M20-2	78.4	19.6	2	0.63	2	3	99.9 ± 1.6
M20-3	77.6	19.4	3	0.63	2	3	109.6 ± 1.6
M20-4	76.8	19.2	4	0.63	2	3	111.3 ± 0.4

flocculation [22]. This process releases water previously trapped within particle clusters, thereby enhancing fluidity.

Following isothermal calorimetry, the ampoules with hydrated pastes were sealed in plastic bags to avoid carbonation and cured at 20 °C and 99 % RH until testing at different ages. Thermogravimetric analysis (Netzsch STA 449 F5 Jupiter) was carried out to quantify portlandite (CH) content using the tangent method at 3 and 28 days [23]. Portlandite content was determined from the mass loss in the temperature range of 400–600 °C using the method described in Ref. [23].

Mineralogy was determined using XRD (Malvern Panalytical Empyrean) with CuKα radiation in a 2 theta range of 5–70 ° and a step size of 0.02°/min. Quantitative XRD was performed using Rietveld analysis with 20 wt% corundum as the internal standard. From the data, the degree of hydration of clinker (DoH) was calculated using equation (1).

$$\text{DoH}\ (\%) = \frac{\sum (C_3S + C_2S + C_3A + C_4AF)_i - \sum (C_3S + C_2S + C_3A + C_4AF)_f}{\sum (C_3S + C_2S + C_3A + C_4AF)_i} \quad (1)$$

Where C_3S, C_2S, C_3A and C_4AF are the normalised mass of the anhydrous phases in the cement paste before (i) and after (f) curing.

2.4. Workability and compressive strength

Seven mortar mixes containing varying amounts of APS (0–40 wt%) and gypsum (0–4 wt%) for 20 wt% APS were prepared at a w/b ratio of 0.63 and sand-to-binder mass ratio of 3. The mixes summarised in Table 3 were used to study the effect of APS on workability and compressive strength. Cement, APS, and river sand (maximum particle size <4 mm with 20 % passing 63 μm sieve) were dry mixed for 2 min. Water and superplasticiser were then added and mixed for 2 min at a slow speed and 3 min at a fast speed. The workability of fresh mortar was measured on a flow table according to BS EN 1015-3. Samples were cast in 50 mm cube steel moulds, compacted on a vibrating table for 3 min and stored in the curing room for 24 h at 99 % relative humidity. They were then demoulded and cured under water for ages of 3, 7, 28 and 90 days. Compressive strength testing was performed on the mortar samples (Instron 5984 universal testing machine) at a loading rate of 0.03 kN/s. Three replicate cubes were tested at each age and averaged.

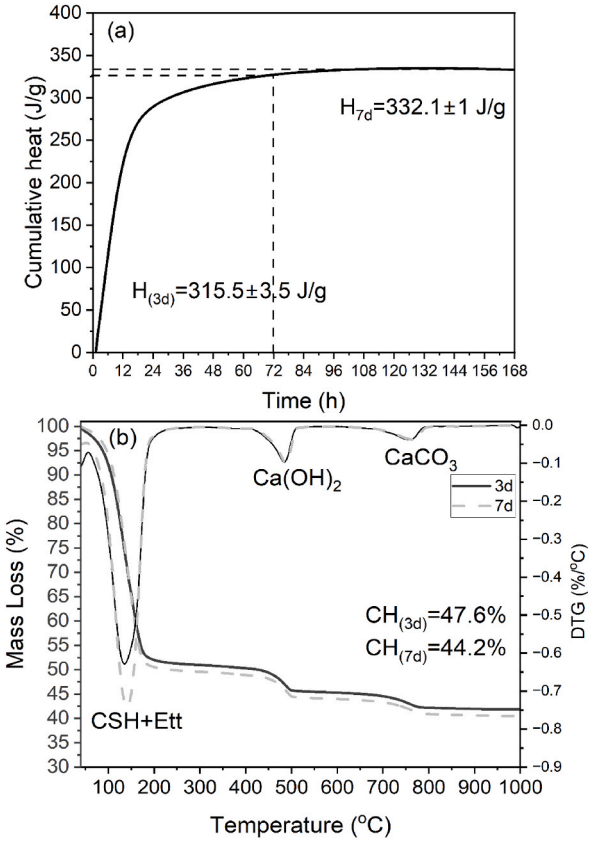

Fig. 2. (a) Cumulative heat evolution and (b) thermogravimetric analysis of the pastes from the R^3 test.

3. Results and discussion

3.1. Pozzolanic reactivity of olivine-derived silica

The cumulative heat release (normalised to the mass of APS) and thermogravimetric analysis of the paste from the R^3 test are shown in Fig. 2a and b, respectively. The cumulative heat of the reaction increases sharply within the first 15 h as a result of the rapid dissolution of APS and calcium hydroxide. This underscores the effectiveness of APS as a reactive SCM. The cumulative heat released rate then slows down and reaches a plateau after ~100 h. The average cumulative heat from three replicates is 315 J/g after 3 days and 332 J/g after 7 days. This exceeds the reactivity threshold value of 160 J/g at a 90 % confidence level as recommended by RILEM TC 267 [24].

The tangent method was used on the thermogravimetric data to quantify mass loss of water corresponding to calcium hydroxide decomposition in the temperature range of 400–600 °C. This was then used to calculate the unreacted calcium hydroxide content expressed as a percentage of the initial amount, giving 47.6 % and 44.2 % at 3 and 7 days, respectively. These results show that little changes occur in the cumulative heat of the reaction or the amount of unreacted calcium hydroxide from 3 to 7 days due to the pozzolanic reaction of silica. This demonstrates that most of the reaction has occurred within the first 3 days of the R^3 test.

To benchmark the reactivity of APS with conventional SCMs, a comparison of the range of 7-day cumulative heat data from the R^3 test method was carried out and presented in Fig. 3. Data for conventional SCMs such as natural pozzolan (NP, volcanic ash), fly ash (PFA), calcined clay (CC), ground granulated blast furnace slag (GGBS), and silica fume (SF) were compiled from the literature and compared against APS from this study. It can be observed that natural pozzolan and PFA tend to achieve lower reactivity, with 7-day cumulative heat values typically below 300 J/g for the majority, compared to APS at ~333 J/g. GGBS displays a broader range, from 350 to 550 J/g, while silica fume and calcined clays often surpass APS, reaching 360–630 J/g and 250–960 J/g at 7 days [24–26]. Thus, the reactivity of APS not only matches but, in some cases, outperforms conventional SCMs, making it a viable candidate as a cement replacement material. These findings position APS as a reactive SCM, with its 7-day cumulative heat comparable or close to the lower end of calcined clay, GGBS and silica fume, and exceeding PFA and natural pozzolan (volcanic ash).

3.2. Influence of APS and sulfate content on hydration kinetics

The isothermal calorimetry results of cement pastes with varying APS content (0–20 wt%), normalised to the mass of cement, are shown in Fig. 4. As expected, the control paste (P0) shows a broad main peak representing the normal reaction of alite (C_3S) followed by the aluminate (C_3A) reaction [27]. However, the blended pastes show a different trend. The presence of APS in P10 and P20 accelerates the aluminate reaction and is ascertained with a prominent aluminate peak that occurs earlier with increasing APS content. The increased cumulative heat released per gram of cement with an increase in APS content indicates that APS contributes to cement hydration both physically (filler or dilution) and chemically (APS dissolution and pozzolanic reaction). The accelerated aluminate hydration is indicated by the sharp increase in the slope of the cumulative heat curves within the first 15h, as shown in Fig. 4b. The earlier onset of aluminate reaction is indicative of rapid sulfate depletion [28,29]. This behaviour has also been observed with other silica-based SCMs, including silica fume and nano silica [30,31]. Cement replacement with SCM promotes C-S-H formation, which accelerates sulfate depletion because of its adsorption onto the C-S-H pore structure [32,33]. Research also reported that SCMs with high specific surface area exacerbate this phenomenon [34]. Thus, the high specific surface area and porous structure of APS have provided additional adsorption sites that fostered sulfate adsorption. The consequence of accelerated sulfate depletion is flash setting and delayed hydration of silicates, which impact mechanical performance. Therefore, more sulfate should be added to compensate for these effects, to delay the aluminate reaction and achieve a good separation between the C_3S and C_3A peaks.

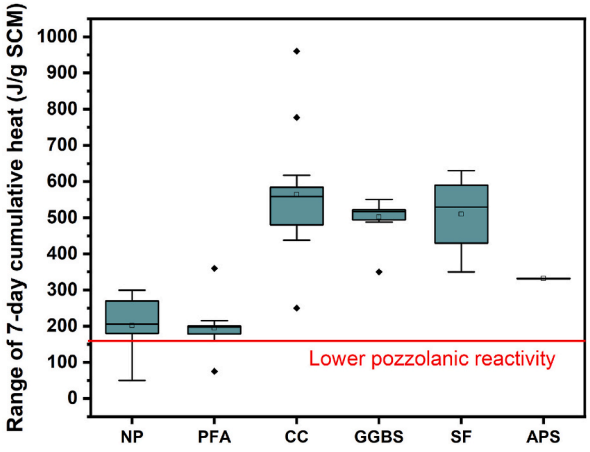

Fig. 3. Comparison of reactivity of conventional SCMs based on the R^3 test 7-day cumulative heat (data reproduced and adapted from Refs. [24–26]) against APS (this study).

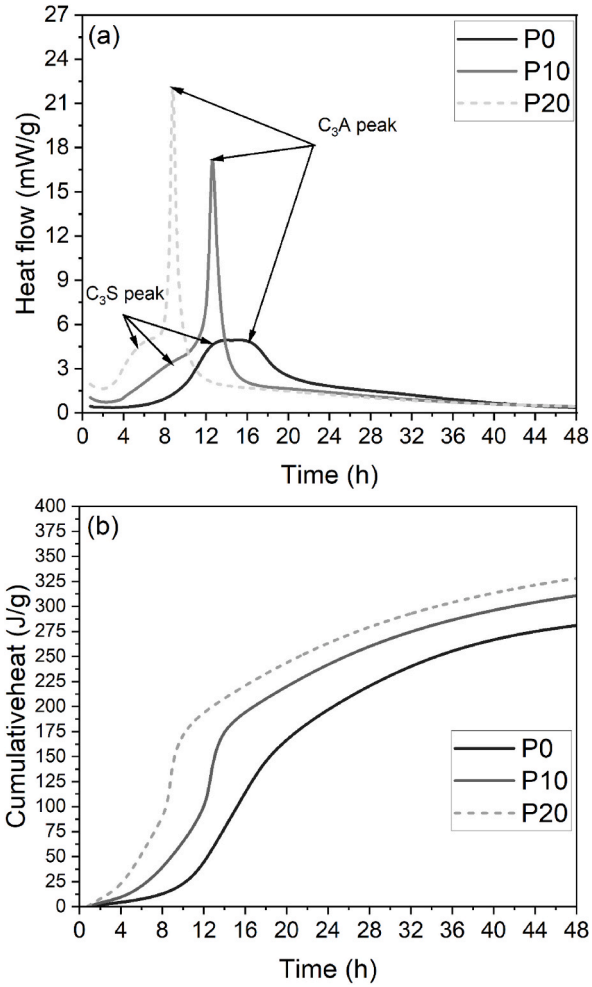

Fig. 4. a) Heat flow and b) cumulative heat of cement pastes with 0, 10 and 20 wt% APS at 0.5 w/b ratio.

To determine the amount of additional sulfate required, tests were carried out by adding gypsum ($CaSO_4.2H_2O$) incrementally to 4 wt%. Fig. 5a depicts the effect of this on the heat of hydration of blended pastes with 20 wt% APS. It is clear that the aluminate peak is delayed and its intensity is greatly reduced with the addition of gypsum. Furthermore, the aluminate peak is well distinguishable from the alite peak. The cumulative heat (Fig. 5b) shows an increase related to the improved dissolution of alite at early ages (<5h), followed by a delay in the aluminate reaction. Furthermore, the cumulative heat of hydration beyond 24h is enhanced. This shows the benefits of sulfate in regulating the hydration of APS blended cement, which is consistent with systems containing other types of SCMs [35,36].

3.3. Phase assemblage and degree of hydration

Table 4 reports the quantitative XRD phase assemblage of hydrated cement paste with varying APS and gypsum content. The hydration of cement phases is enhanced with curing age. However, the hydration of C_3S and C_2S is reduced with increased APS content. Furthermore, APS increases ettringite formation due to the accelerated C_3A reaction induced by sulfate depletion. The dissolution of C_3A releases aluminium ions, which react with sulfate and calcium to form ettringite [37]. The presence of finely divided SCMs with high surface area, such as APS, provides nucleation sites that reduce ettringite conversion to monosulfate [38,39]. Therefore, ettringite is stabilised at high contents of APS even as sulfate is rapidly depleted. Portlandite content decreases with an increase in APS content, and with curing age for mixes containing 20 wt% APS. This is due to the cement dilution effect and the pozzolanic reaction induced by APS.

The addition of 2–4 wt% gypsum to P20 increases the hydration of C_3S and C_2S due to the delayed aluminate reaction. However, the amount of portlandite remaining after 28 days of hydration does not change significantly because of the constant APS content in these mixes. Ettringite formation is increased with additional gypsum because more sulfate ions are present to react with the aluminate species. AFm decreases with curing age, but there is no clear distinction between mixes with different APS contents. Gypsum addition

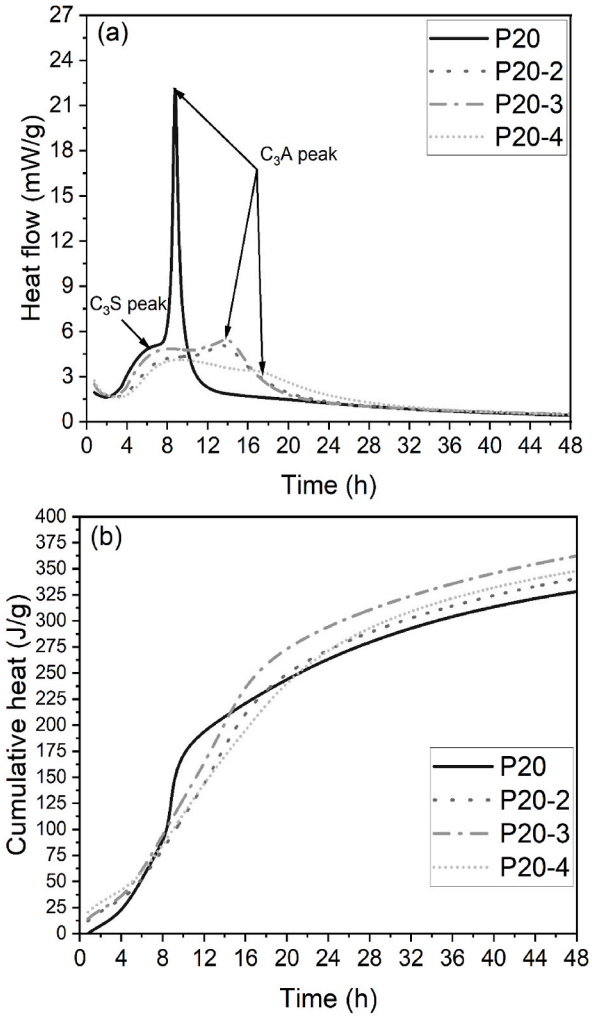

Fig. 5. a) Heat flow and b) cumulative heat of blended cement paste with 20 wt% APS and varying additional gypsum (0–4 wt%) at 0.5 w/b ratio.

Table 4
Phase assemblage (in g per 100 g of cement) of anhydrous clinker, and hydrated cement phases from pastes at varying APS content (0–20 wt%) and gypsum addition (0–4 wt%) with 20 wt% APS at 0.5 w/b ratio.

Phase	3 days						28 days					
	P0	P10	P20	P20-2	P20-3	P20-4	P0	P10	P20	P20-2	P20-3	P20-4
Portlandite	13.2	10.5	6.6	2.5	2.4	2.1	14.7	12	3	2.5	2.8	1.9
Ettringite	7.8	11.2	18.2	11.8	18.1	17.2	7.3	11.2	12.6	16.6	18.1	18.5
AFm	1.5	1.5	1.5	0.6	0.6	0.2	0.9	1.1	0.6	0.4	0.4	0.2
C_3S	5.2	8	13.1	5.2	5	7.1	1.9	1.3	4.5	2.7	3	3.3
C_2S	5.1	7	9.2	3.3	6.4	3.9	4.3	5.8	5.4	4.4	5.6	3.5
C_3A	0.0	0.0	0.0	0.0	0.0	0.0	0.0	0.0	0.0	0.0	0.0	0.0
C_4AF	0.0	0.0	0.0	0.0	0.4	0.0	0.0	0.0	0.0	0.0	0.0	0.0

decreases AFm slightly in favour of ettringite. However, AFm phases, especially the dominant sulfate-AFm form, are very difficult to detect accurately through XRD because of low crystallinity.

The XRD data of 28-day hydrated cement paste at varying APS content (0–20 wt%) and gypsum addition (0–4 wt%) in the range of 8–20° (2θCuKα) are shown in Fig. 6. Peaks of ettringite, portlandite and AFm (monosulfate, hemicarbonate and monocarbonate) are detected as the main crystalline hydrated phases. AFm phases are major reaction products of aluminates in cement via the transformation of ettringite [40]. The dominant form is sulfate-AFm, which can transform into carbonate-AFm phases due to atmospheric carbonation or in the presence of calcium carbonate. The diffractograms revealed the presence of hemicarbonate and monocarbonate in all samples except P20, where monocarbonate is absent (Fig. 6a). The presence of calcite in anhydrous cement is likely to promote

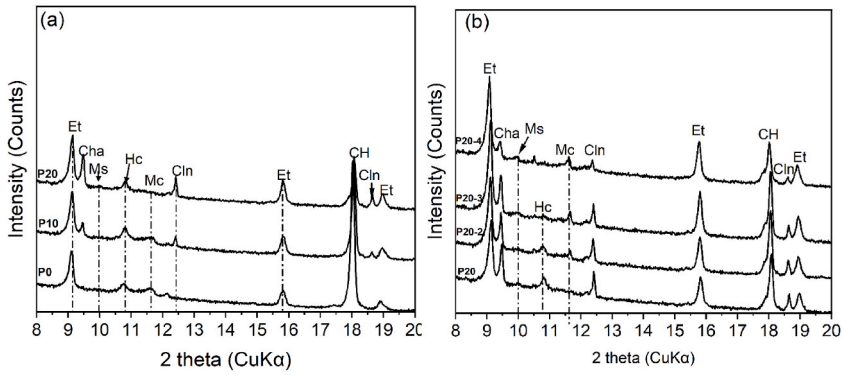

Fig. 6. XRD patterns of 28-day hydrated cement paste at varying a) APS content (0–20 wt%) and b) gypsum addition (0–4 wt%) with 20 wt% APS. Notation: Ett = ettringite; Ms = monosulfate; Hc = hemicarbonate; Mc = monocarbonate; CH = portlandite; Cln = clinochlore; Cha = chabazite.

the formation of carbonate-AFm. The addition of gypsum modifies the AFm phases by promoting the formation of monosulfate and monocarbonate (Fig. 6b). In contrast, the peak intensity for hemicarbonate decreases and almost disappears at 4 wt% gypsum addition.

The degree of hydration (DoH) of clinker phases with curing age is shown in Fig. 7. As expected, the degree of hydration increases considerably with curing age but decreases with APS content at 3 and 28 days. The decrease is more prominent at 3 days and stems from the hindrance of the alite and belite hydration as shown by QXRD results (Table 4). This trend is also due to the rapid sulfate depletion, as demonstrated by the calorimetry data, where hydration of silicate phases is hindered by the early reaction of aluminates. Addition of gypsum to the mix with 20 wt% APS accelerated DoH at 3 and 28 days, which became comparable to the control cement paste (P0) and surpassed the benchmark (P20) without gypsum. That is ascribed to the delayed aluminates hydration along with the filler effect that enhances the silicates reaction.

3.4. Thermogravimetry analysis

Figs. 8 and 9 show the differential thermogravimetry (DTG) of hydrated cement pastes at 3 and 28 days with varying APS content (0–20 wt%) and gypsum addition (0–4 wt%) for 20 wt% APS. The major mass loss before 250 °C corresponds to the decomposition of C-S-H, ettringite and AFm. The partial substitution of cement with APS decreases the formation of AFm, due to ettringite stabilization as discussed previously. The addition of gypsum (Fig. 9) increases the mass loss associated with the decomposition of C-S-H and ettringite. However, AFm is barely discernible on P20-2, P20-3 and P20-4. Finally, one can also observe the decomposition of clinochlore from unreacted APS and the decomposition of calcite present from the unreacted cement or carbonation of hydrated phases.

Fig. 10 shows the changes in CH content in the hydrated cement pastes, determined from thermogravimetric analysis. CH content increases with curing time due to the continuous hydration of the cement phases as described earlier. CH content in the blended cement pastes decreases with an increase in APS content as a consequence of both the cement dilution effect and the pozzolanic reaction. Additional gypsum to P20 does not change the CH content irrespective of the gypsum content. These trends agree with the QXRD results presented earlier.

3.5. Workability and compressive strength

Flow table data on mortars at a w/b ratio of 0.63 and a sand-to-binder mass ratio of 3 are reported in Table 3. The control sample M0 has a flow of 163 mm. Flow decreases to 100 mm for 40 wt% APS replacement. The addition of gypsum slightly improves the flowability to 111 mm because of a filler effect and the delayed aluminate reaction as described previously. The smaller flow recorded for M-20-2 might be due to an artefact during measurement.

The influence of APS and gypsum addition (for 20 wt% APS) on compressive strength evolution is shown in Fig. 11. In general, compressive strength increases with curing age. At early ages of 3 and 7 days, the blended mortars developed lower strength than the control M0. At later ages, compressive strength of the blended mortars increases significantly with APS content up to 20 wt%, achieving comparable values to the control at 28 days and higher at 90 days. However, 40 wt% replacement leads to lower strength at all ages.

The effect of APS on strength evolution can be explained by the reaction mechanism prevailing at early and late ages. Although the R^3-test showed increased cumulative heat at early ages (Fig. 2), the delayed hydration of silicates leads to lower strength. Furthermore, the dilution effect of APS is dominant at early ages, along with the physical sorption of sulfate. This also explains the significant strength loss at a higher replacement level (40 wt%), where no portlandite is identified from an early age (supplementary file, S1). At later ages, the rapid strength increase with APS content up to 20 wt% is ascribed to the pozzolanic reaction, which consumes portlandite to form additional C-S-H, as confirmed with QXRD and TGA.

The addition of gypsum helps to correct the reaction mechanism at early ages by promoting the filler effect, delaying the aluminate reaction and improving the silicates hydration. This is demonstrated by isothermal conduction calorimetry, QXRD and the enhanced

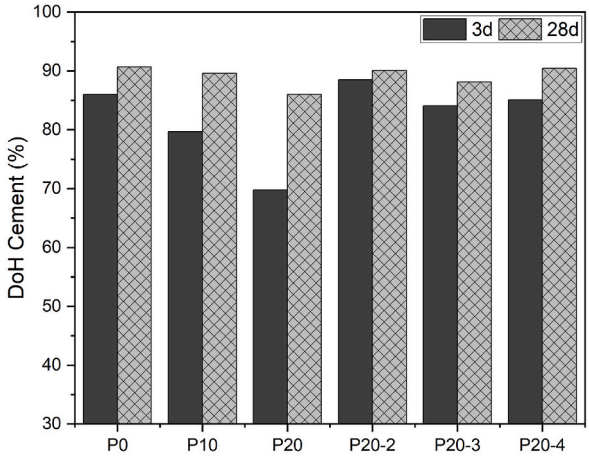

Fig. 7. Degree of hydration of cement with varying APS content (0–20 wt%) and gypsum addition (0–4 wt%) after 3 and 28 days.

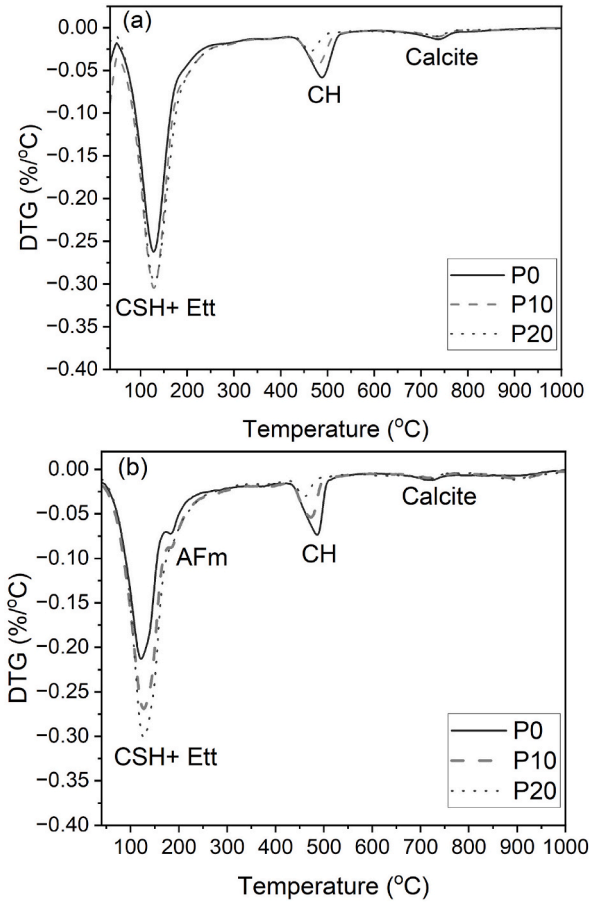

Fig. 8. Differential thermogravimetry (DTG) of cement pastes with varying APS content (0–20 wt%) at a) 3 days and b) 28 days.

degree of hydration at 3 days (Fig. 7), which improves early age compressive strength (Fig. 11). The strength at later ages (28 and 90 days) does not change considerably with gypsum content. This is consistent with the low variation in CH content (Table 4 and Fig. 10) for samples with additional gypsum (P20-2, P20-3 and P20-4). This shows that the filler effect of gypsum is favourable for early-age hydration and does not contribute to promoting pozzolanic reaction beyond 7 days, as discussed previously.

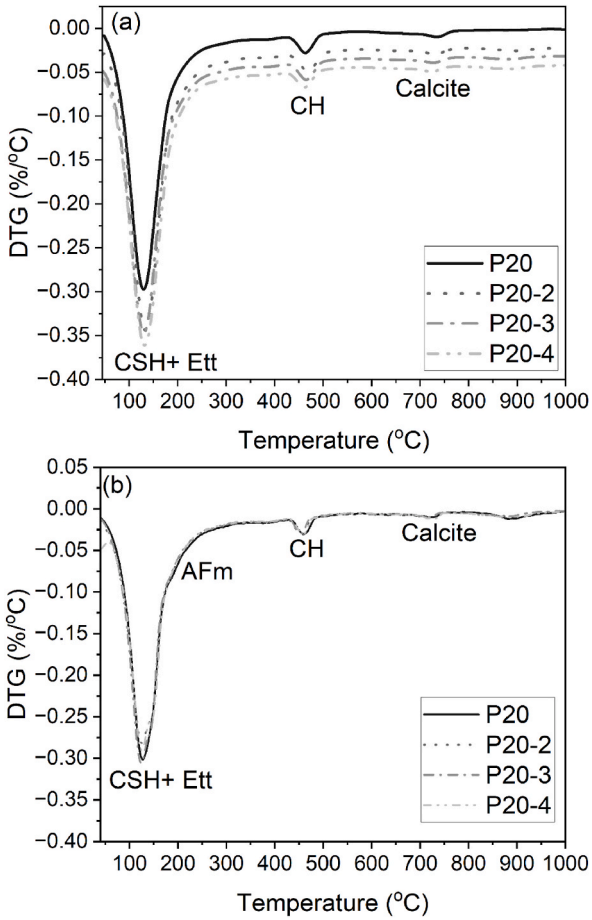

Fig. 9. Differential thermogravimetry (DTG) of cement pastes with varying gypsum addition (0–4 wt%) for 20 wt% APS at a) 3 days and b) 28 days.

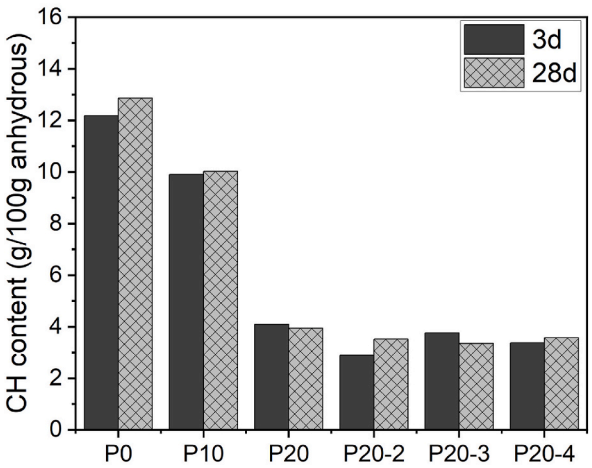

Fig. 10. Portlandite content of cement pastes at different APS (0–20 wt%) and gypsum addition (0–4 wt%) determined from TGA.

4. Conclusion

The reactivity of olivine-derived amorphous precipitated silica (APS) as SCM in blended cement is reported. The work has investigated the interactions between APS and cement hydration in the presence of sulfate and the influence this has on reaction kinetics, phase assemblage, workability and strength development. The main findings are summarised as follows:

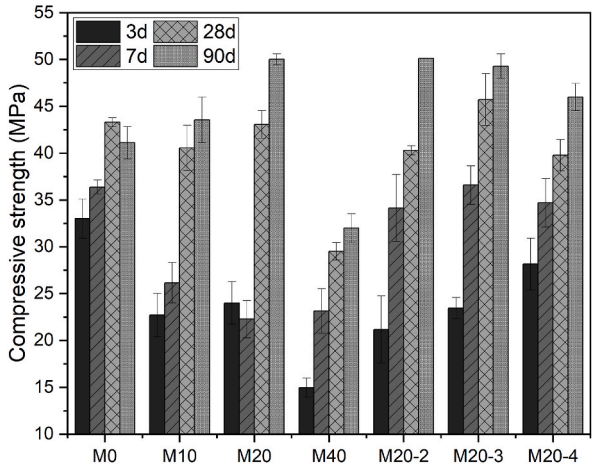

Fig. 11. Compressive strength evolution of mortars at 0.63 w/b with different APS content (0–40 wt%) and gypsum addition (0–4 wt%) for 20 wt % APS.

i) APS achieves an R^3 cumulative heat of 315 J/g after 3 days and 333 J/g after 7 days. This exceeds the reactivity threshold value of 160 J/g at 90 % confidence level according to RILEM TC 267.
ii) APS is a fine material with a porous structure and high specific surface area (168 m^2/g) that increases the water demand and significantly reduces the workability of cement-based materials.
iii) APS accelerates sulfate depletion, which increases the C_3A reaction. APS also provides nucleation sites for ettringite formation, and this increases ettringite content.
iv) Partial replacement of Portland cement with APS induces a dilution effect, which delays hydration and decreases compressive strength at early ages. Pozzolanic reaction becomes the dominant mechanism at later ages, with significant improvement in compressive strength that outperforms the control cement mortar.
v) Addition of excess gypsum (2–4 wt%) promotes a filler effect-dominated reaction mechanism at early ages, resulting in enhancement of hydration and compressive strength, which exceeds that of the control cement mortar.
vi) The optimal use of APS as SCM requires a CEM I replacement level of a maximum of 20 wt% with an additional gypsum content of 2–3 wt%.

CRediT authorship contribution statement

Jean Noel Yankwa Djobo: Writing – review & editing, Writing – original draft, Methodology, Investigation, Formal analysis, Conceptualization. **Sam Draper:** Writing – review & editing, Investigation. **Barney Shanks:** Writing – review & editing, Investigation. **Hong Wong:** Writing – review & editing, Writing – original draft, Supervision, Resources, Funding acquisition. **Christopher Cheeseman:** Writing – review & editing, Supervision, Resources, Funding acquisition.

Declaration of competing interest

The authors declare the following financial interests/personal relationships which may be considered as potential competing interests:Chris Cheeseman reports financial support was provided by Department for Energy Security and Net Zero (DESNZ), UK. If there are other authors, they declare that they have no known competing financial interests or personal relationships that could have appeared to influence the work reported in this paper.

Acknowledgement

This work was funded by the Department for Energy Security and Net Zero (DESNZ), under project number CCUS 2106 of the CCUS Innovation 2.0 call – part of the Net Zero Innovation Portfolio (NZIP). The research leading to this publication benefited from UKCRIC Advanced Infrastructure Materials Laboratory funding under grant no. EP/R010161/1 and support from the UKCRIC Coordination Node, EPSRC grant no. EP/R017727/1, which funds UKCRIC's ongoing coordination.

Appendix A. Supplementary data

Supplementary data to this article can be found online at https://doi.org/10.1016/j.jobe.2025.114379.

Data availability

Data will be made available on request.

References

[1] United Nations Environment Programme, Building material and the climate: constructing a new future, Nairobi (2023), https://doi.org/10.59117/20.500.11822/43293.
[2] United Nations Environment Programme, Global status report for buildings and construction: beyond foundations - mainstreaming sustainable solutions to cut emissions from the buildings sector, Nairobi (2023), https://doi.org/10.59117/20.500.11822/45095, 2024.
[3] I.H. Shah, S.A. Miller, D. Jiang, R.J. Myers, Cement substitution with secondary materials can reduce annual global CO2 emissions by up to 1.3 gigatons, Nat. Commun. 13 (2022) 1–11, https://doi.org/10.1038/s41467-022-33289-7.
[4] X. Li, J. Dengler, C. Hesse, Reducing clinker factor in limestone calcined clay-slag cement using C-S-H seeding – a way towards sustainable binder, Cement Concr. Res. 168 (2023) 107151, https://doi.org/10.1016/j.cemconres.2023.107151.
[5] T.C. Cardoso, P.R. de Matos, L. Py, M. Longhi, O. Cascudo, A.P. Kirchheim, Ternary cements produced with non-calcined clay, limestone, and Portland clinker, J. Build. Eng. 45 (2022) 103437, https://doi.org/10.1016/j.jobe.2021.103437.
[6] K.H. Yang, G.D. Moon, Y.S. Jeon, Implementing ternary supplementary cementing binder for reduction of the heat of hydration of concrete, J. Clean. Prod. 112 (2016) 845–852, https://doi.org/10.1016/j.jclepro.2015.06.022.
[7] S. Kumar, J.N.Y. Djobo, A. Kumar, S. Kumar, Size fractionation of brown fly ash: utilisation of grey fraction as a pozzolanic material in blended cement, Eur. J. Environ. Civ. Eng. 24 (2020), https://doi.org/10.1080/19648189.2018.1427635.
[8] J. Yoon, K. Jafari, R. Tokpatayeva, S. Peethamparan, J. Olek, F. Rajabipour, Characterization and quantification of the pozzolanic reactivity of natural and non-conventional pozzolans, Cem. Concr. Compos. 133 (2022) 104708, https://doi.org/10.1016/j.cemconcomp.2022.104708.
[9] B. Shanks, C. Howe, S. Draper, H. Wong, C. Cheeseman, Carbon capture and storage in low-carbon concrete using products derived from olivine, R. Soc. Open Sci. 11 (2024), https://doi.org/10.1098/rsos.231645.
[10] B. Shanks, C. Howe, S. Draper, H. Wong, C. Cheeseman, Production of low-carbon amorphous SiO2 for use as a supplementary cementitious material and nesquehonite from olivine, Mater. Lett. 361 (2024) 136133, https://doi.org/10.1016/j.matlet.2024.136133.
[11] D. Meng, C. Unluer, E.H. Yang, S. Qian, Recent advances in magnesium-based materials: CO2 sequestration and utilization, mechanical properties and environmental impact, Cem. Concr. Compos. 138 (2023) 104983, https://doi.org/10.1016/J.CEMCONCOMP.2023.104983.
[12] A. Scott, C. Oze, V. Shah, N. Yang, B. Shanks, C. Cheeseman, A. Marshall, M. Watson, Transformation of abundant magnesium silicate minerals for enhanced CO2 sequestration, Commun. Earth Environ. 2 (2021) 1–6, https://doi.org/10.1038/s43247-021-00099-6.
[13] S. Allan Nye, S. Vineet, O. Christopher, S. Barnaby, C. Chris, Use of olivine for the production of MgO-SiO2 binders, Front. Built Environ. 7 (2021) 1–8, https://doi.org/10.3389/fbuil.2021.640243.
[14] R. Michel, M.R. Ammar, J. Poirier, P. Simon, Phase transformation characterization of olivine subjected to high temperature in air, Ceram. Int. 39 (2013) 5287–5294, https://doi.org/10.1016/j.ceramint.2012.12.031.
[15] I.A. Munz, J. Kihle, Ø. Brandvoll, I. Machenbach, J.W. Carey, T.A. Haug, H. Johansen, N. Eldrup, A continuous process for manufacture of magnesite and silica from olivine, CO2 and H2O, Energy Proc. 1 (2009) 4891–4898, https://doi.org/10.1016/j.egypro.2009.02.319.
[16] N. Raza, W. Raza, S. Madeddu, H. Agbe, R.V. Kumar, K.H. Kim, Synthesis and characterization of amorphous precipitated silica from alkaline dissolution of olivine, RSC Adv. 8 (2018) 32651–32658, https://doi.org/10.1039/c8ra06257a.
[17] V. Shah, A. Scott, Pozzolanic characteristics of silica recovered from olivine, Constr. Build. Mater. 332 (2022) 127378, https://doi.org/10.1016/j.conbuildmat.2022.127378.
[18] A. Lazaro, H.J.H. Brouwers, G. Quercia, J.W. Geus, The properties of amorphous nano-silica synthesized by the dissolution of olivine, Chem. Eng. J. 211–212 (2012) 112–121, https://doi.org/10.1016/j.cej.2012.09.042.
[19] T. Oh, B. Chun, S.K. Lee, G.W. Kim, N. Banthia, D.-Y. Yoo, Effect of high-volume substituted nanosilica on the hydration and mechanical properties of ultra-high-performance concrete (UHPC), Cement Concr. Res. 175 (2024) 107379, https://doi.org/10.1016/j.cemconres.2023.107379.
[20] L.G. Py, J.S.A. Neto, M.A. Longhi, A.P. Kirchheim, Evaluation of ultrafine calcined clays on LC3 cements on the sulfate requirement, water demand and strength development, Mater. Struct. Constr. 57 (2024), https://doi.org/10.1617/s11527-023-02288-5.
[21] ASTM C1897-20, Standard Test Methods for Measuring the Reactivity of Supplementary Cementitious Materials by Isothermal Calorimetry and Bound Water Measurements, 4, ASTM Int. West, Conshohocken, PA, 2020, pp. 7–11, https://doi.org/10.1520/C1897-20.2.
[22] P.C. Nkinamubanzi, S. Mantellato, R.J. Flatt, Superplasticizers in Practice, Elsevier Ltd, 2016, https://doi.org/10.1016/B978-0-08-100693-1.00016-3.
[23] K. Scrivener, R. Snellings, B. Lothenbach, A Practical Guide to Microstructural Analysis of Cementitious Materials, CCR Press, 2016, https://doi.org/10.1201/b19074.
[24] D. Londono-Zuluaga, A. Gholizadeh-Vayghan, F. Winnefeld, F. Avet, M. Ben Haha, S.A. Bernal, Ö. Cizer, M. Cyr, S. Dolenec, P. Durdzinski, J. Haufe, D. Hooton, S. Kamali-Bernard, X. Li, A.T.M. Marsh, M. Marroccoli, M. Mrak, Y. Muy, C. Patapy, M. Pedersen, S. Sabio, S. Schulze, R. Snellings, A. Telesca, A. Vollpracht, G. Ye, S. Zhang, K.L. Scrivener, Report of RILEM TC 267-TRM phase 3: validation of the R3 reactivity test across a wide range of materials, Mater. Struct. 55 (2022), https://doi.org/10.1617/s11527-022-01947-3.
[25] R. Snellings, P. Suraneni, J. Skibsted, Future and emerging supplementary cementitious materials, Cement Concr. Res. 171 (2023) 107199, https://doi.org/10.1016/j.cemconres.2017.08.015.
[26] R. Snellings, D. Londoño-Zuluaga, K. Scrivener, Interlaboratory test program to determine the precision of the R3 test method (ASTM C1897-20) for measuring reactivity of supplementary cementitious materials, Adv. Civ. Eng. Mater. 11 (2022), https://doi.org/10.1520/ACEM20220023.
[27] H.F.W. Taylor, Cement Chemistry, second ed., Thomas Telford Publishing, London, 1997 https://doi.org/10.1680/cc.25929.
[28] O. Canbek, C. Szeto, N.R. Washburn, K.E. Kurtis, A quantitative approach to determining sulfate balance for LC3, Cemento 12 (2023) 100063, https://doi.org/10.1016/j.cement.2023.100063.
[29] K. Scrivener, F. Avet, H. Maraghechi, F. Zunino, J. Ston, W. Hanpongpun, A. Favier, Impacting factors and properties of limestone calcined clay cements (LC3), Green Mater. 7 (2018) 3–14, https://doi.org/10.1680/jgrma.18.00029.
[30] G. Quercia, H.J.H. Brouwers, A. Garnier, K. Luke, Influence of olivine nano-silica on hydration and performance of oil-well cement slurries, Mater. Des. 96 (2016) 162–170, https://doi.org/10.1016/j.matdes.2016.02.001.
[31] F. Lavergne, R. Belhadi, J. Carriat, A. Ben Fraj, Effect of nano-silica particles on the hydration, the rheology and the strength development of a blended cement paste, Cem. Concr. Compos. 95 (2019) 42–55, https://doi.org/10.1016/j.cemconcomp.2018.10.007.
[32] J. da S. Andrade Neto, A.G. De la Torre, A.P. Kirchheim, Effects of sulfates on the hydration of Portland cement – a review, Constr. Build. Mater. 279 (2021), https://doi.org/10.1016/j.conbuildmat.2021.122428.
[33] Y. Dhandapani, A.T.M. Marsh, S. Rahmon, F. Kanavaris, A. Papakosta, S.A. Bernal, Suitability of excavated London clay as a supplementary cementitious material: mineralogy and reactivity, Mater. Struct. Constr. 56 (2023) 1–21, https://doi.org/10.1617/s11527-023-02260-3.
[34] F. Zunino, K. Scrivener, The influence of the filler effect on the sulfate requirement of blended cements, Cement Concr. Res. 126 (2019) 105918, https://doi.org/10.1016/j.cemconres.2019.105918.
[35] M. Rubens, S. Andrade, B. Walkley, A. Paula, Exploring sulfate optimization techniques in limestone calcined clay cements (LC 3): limitations and insights, Cement Concr. Res. 175 (2024) 107375, https://doi.org/10.1016/j.cemconres.2023.107375.
[36] S. Adu-Amankwah, L. Black, J. Skocek, M. Ben Haha, M. Zajac, Effect of sulfate additions on hydration and performance of ternary slag-limestone composite cements, Constr. Build. Mater. 164 (2018) 451–462, https://doi.org/10.1016/j.conbuildmat.2017.12.165.

[37] K.L. Scrivener, A. Nonat, Hydration of cementitious materials, present and future, Cement Concr. Res. 41 (2011) 651–665, https://doi.org/10.1016/j.cemconres.2011.03.026.
[38] J.W. Bullard, H.M. Jennings, R.A. Livingston, A. Nonat, G.W. Scherer, J.S. Schweitzer, K.L. Scrivener, J.J. Thomas, Mechanisms of cement hydration, Cement Concr. Res. 41 (2011) 1208–1223, https://doi.org/10.1016/j.cemconres.2010.09.011.
[39] B. Lothenbach, K. Scrivener, R.D. Hooton, Supplementary cementitious materials, Cement Concr. Res. 41 (2011) 1244–1256, https://doi.org/10.1016/j.cemconres.2010.12.001.
[40] I. Odler, Hydration, setting and hardening of Portland cement, Lea's Chem. Cem. Concr. (2003) 241–297, https://doi.org/10.1016/B978-075066256-7/50018-7.